Hyperon Acceptance Studies with the CLAS

Philip L. Cole

January 1992

Abstract

We study the geometrical acceptances and mass reconstruction efficiencies of photoproduced hyperons and kaons in the CLAS detector in Hall B. This study was undertaken to support the feasibility of measuring strange particles produced in nuclei with the tagged photon beam. The techniques developed herein for identifying strange particles are nearly independent of target and can equally as well be applied to (e,e'KY) events.

Contents

List of Figures

List of Tables

1 Introduction

In this CLAS note, we discuss the acceptance and mass reconstruction efficiencies of hyperons for the reactions N(γ,KY), where N denotes the nucleon within a fermi gas distribution and Y represents either the isospin singlet Λ^0 or one of the three I = 1 hyperons (Σ^-, Σ^0 or Σ^+). The program GAMMA_K [1] generated the photoproduced quasi-free strange events and these events were, in turn, fed into the CLAS detector simulation package, FASTMC [2]. We vary the incident photon energy and the magnitude and polarity of the magnetic field to ascertain the optimum operating point for kaon-hyperon acceptance.

The techniques developed herein for accepting the photoproduced hyperons and kaons do not depend upon whether the incident photon is real or virtual. This CLAS-NOTE is therefore useful for experiments involving (e,e'KY) events. Moreover, our techniques for identifying strange events are nearly A independent, i.e. it doesn't matter if the target is deuterium or iron.

2 Event Generator

The event generator, GAMMA_K, produces the reactions:

- $\gamma + p \rightarrow \mathrm{K}^+ + \Lambda^0$
- $\gamma + p \rightarrow \mathrm{K}^+ + \Sigma^0$
- $\gamma + n \rightarrow \mathrm{K}^+ + \Sigma^-$
- $\gamma + n \rightarrow \mathrm{K}^0 + \Lambda^0$
- $\gamma + n \rightarrow \mathrm{K}^0 + \Sigma^0$
- $\gamma + p \rightarrow \mathrm{K}^0 + \Sigma^+$

The distribution of nucleons adheres to the fermi-gas model. In generating the target nucleon energy, the nucleon momentum p is picked at random, where the energy of the nucleon is given by the relationship:

$$E_{\mathrm{N}} = \sqrt{M_{\mathrm{N}}^2 + |\vec{p}|^2} + U_0 \qquad (1)$$

Here, the potential energy, U_0, is chosen to be -30 MeV at the bottom of the fermi sea[1]. If the invariant mass of incident photon and the target nucleon exceeds threshhold, the event is kept. The corresponding 4-momenta of the outgoing strange particles are generated at random in the center of mass frame with the constraint that both the total momentum and energy are conserved.

3 Detector Simulation

The next link in the chain of our acceptance studies was to simulate a realistic rendering of the geometry and mass distribution of the CLAS detector. We used the standard Hall B FASTMC parametric Monte Carlo. FASTMC includes such effects as particle decay, dE/dX losses, detector efficiencies and geometrical acceptance. FASTMC allows the user to select such input parameters as the strength and polarity of the magnetic field, RMS width of the beam, size and type of target. Further details can be found in Ref. [2]. A side view of the detector layout is illustrated in Fig. 1.

4 Acceptance and Mass Reconstruction Efficiency

We define the acceptance in the usual way:

$$\varepsilon = \frac{N_{\rm acc}}{N_{\rm gen}}$$

where $N_{\rm gen}$ is the total number of events generated and $N_{\rm acc}$ represents the number of events accepted after passing all cuts. Furthermore, the acceptance, ε, depends upon the incident tagged photon energy, E_γ, and upon both the strength and polarity of the toroidal field of the CLAS. Quantitatively:

$$\varepsilon = \varepsilon(\mathrm{E}_\gamma, \vec{B})$$

For this study, between 36000 and 50000 events were generated for each bin. We binned the acceptance in terms of:

1. E_γ: The energy of the tagged photon beam was discretely binned at 1.2, 1.5 and 1.8 GeV.
2. B field: The magnetic field was set to 0.1, 0.25, 0.50 and 0.75 nominal strength. (For the $\mathrm{K}^+\mathrm{Y}$ channels, we included reversed field bins).

[1]The average energy of a nucleon is the sum of the mean kinetic and potential energies, $U_0 + \frac{3}{5}E_{\rm fermi}$, where $E_{\rm fermi} = p^2_{\rm fermi}/2M$. Setting $p_{\rm fermi}$ to 200 MeV and U_0 to -30 MeV, gives an average binding energy of around -18 MeV [3].

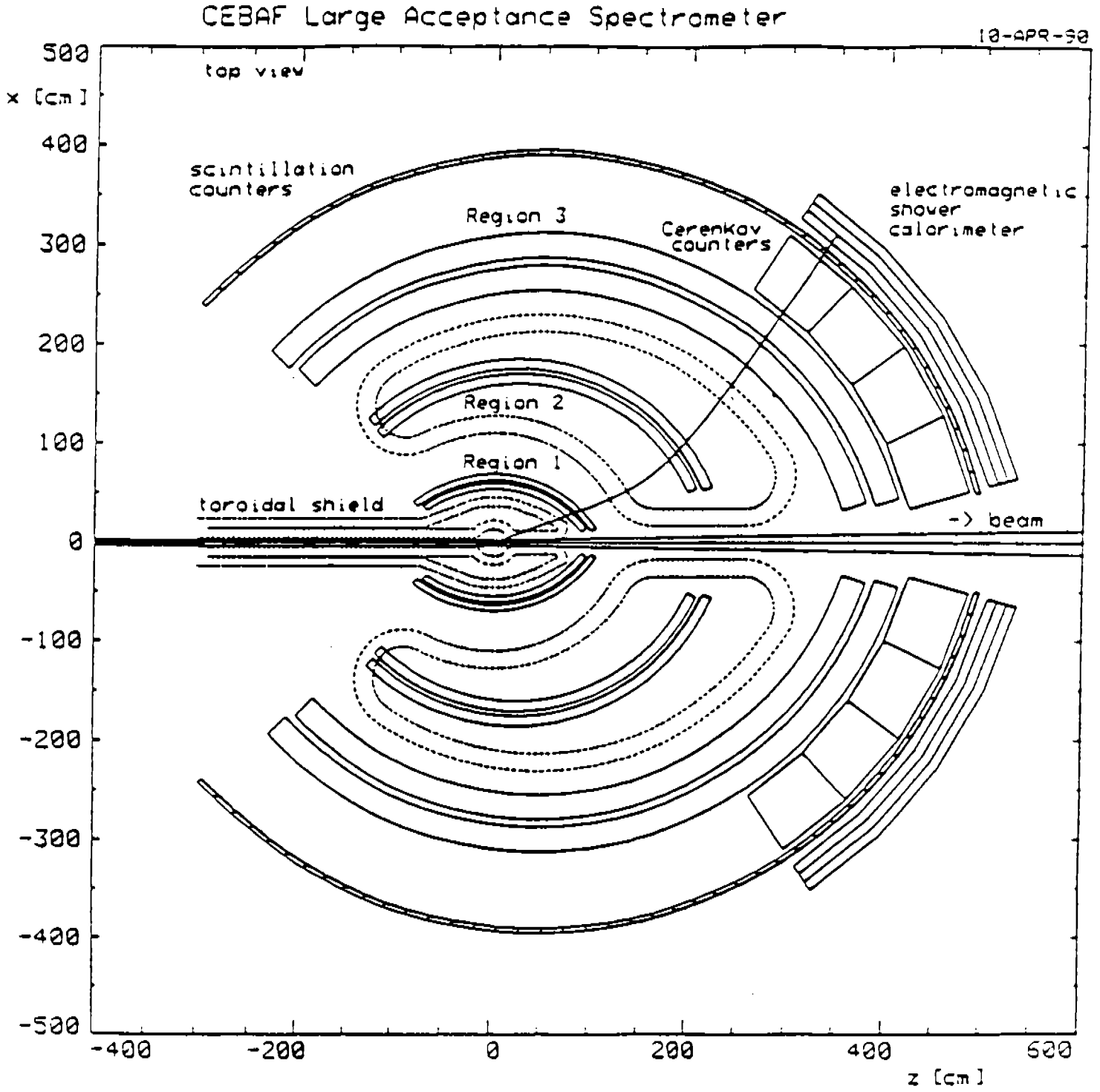

Figure 1: Side view of CLAS detector, which includes three drift chamber regions (I, II & III), the Čerenkov counters, time of flight scintillators and electromagnetic shower counters.

We chose the following input parameters for the FASTMC detector simulation:

1. No Vertexing: The track reconstruction does not include the target as a vertex.
2. Error in momentum: Positional mismeasurement and multiple scattering terms included.
3. Beam: RMS width of photon beam set to 1 cm.
4. Target: ^{12}C. For other targets, U_0 and p_{fermi} (eqn. 1) will have be changed to account for differing binding energies.

Each job, binned in terms of photon energy and magnetic field, consumed approximately 12 VAX 11/780 equivalent CPU hours. We processed 108 jobs which provides a Monte Carlo sample of over 4.5 million events.

4.1 Momentum Resolution

The momentum resolution depends upon such quantities as the particle velocity, the direction and strength of the magnetic field, the particle type and and how well the particle was tracked. For example, not including region III in the tracking degrades the momentum resolution by a factor of four. In Figs. 2(a) through 2(c) we show the momentum resolution for the π^+, π^- and the proton for a positive polarity magnetic field at half strength. As will be made clear in subsection 4.3, we demand that the pions make it only through region II. The protons, however, must be tracked through all three regions and have also deposited energy in a TOF counter[2].

4.2 Particle ID

For a particle that is tracked through regions I, II & III and deposits energy in a TOF counter, we can calculate its mass from the relativistic relationship:

$$m^2 = p^2 \frac{1-\beta^2}{\beta^2}$$

where

$$\beta = \frac{1}{c}\frac{\ell}{\Delta t}$$

[2]It is absolutely necessary to tag the proton for Λ^0 and Σ^0 polarization studies.

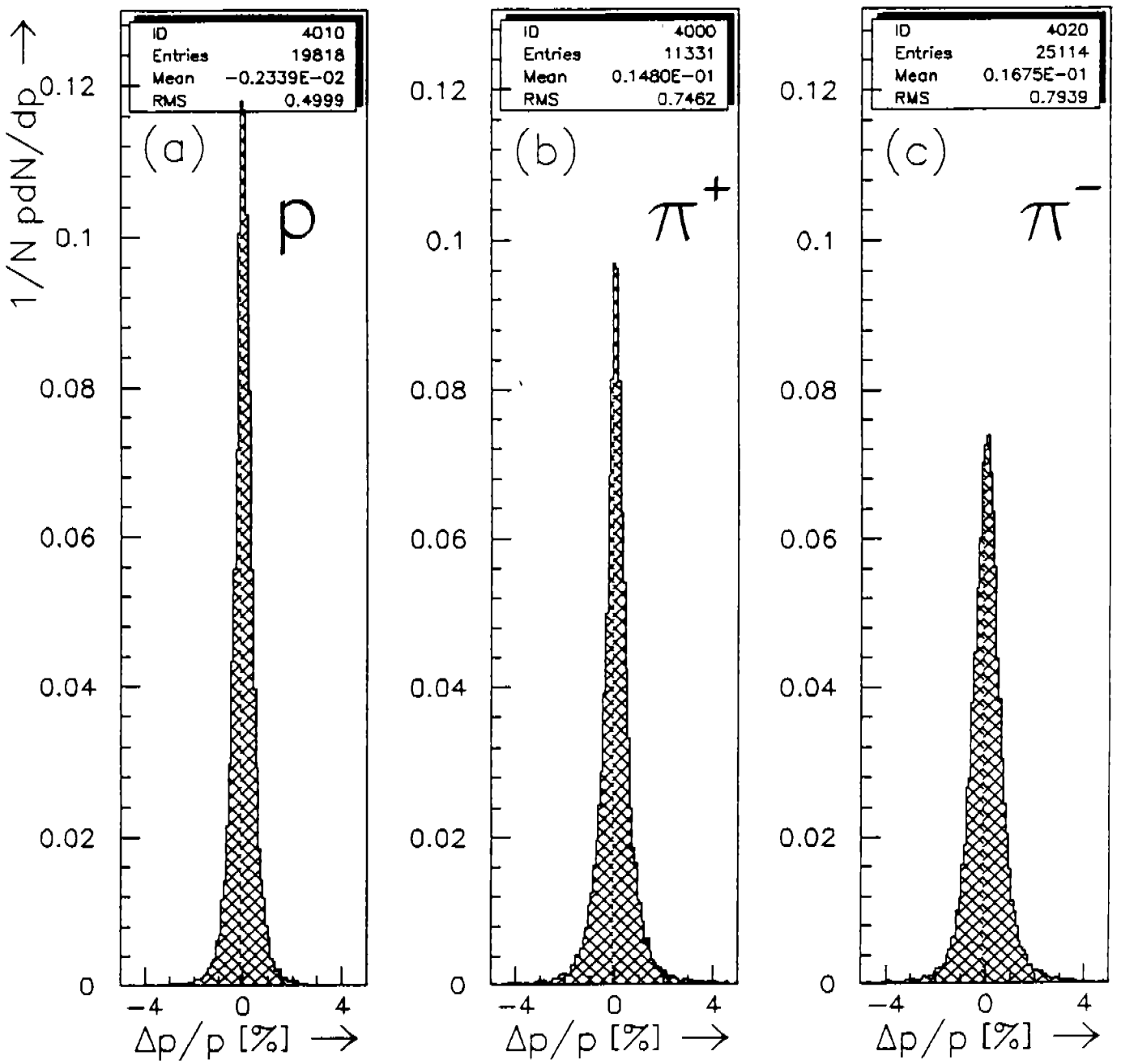

Figure 2: Momentum resolution of (a) protons (b) π^+s and (c) π^-s produced from the reaction $\gamma + n \rightarrow K^0 + \Sigma^0$. B = $+0.5B_0$ and $K^0_S \rightarrow \pi^+\pi^-$ (68.6%) & $\Lambda^0 \rightarrow p\pi^-$ (64.1%).

Table 1: Particle identification.

Particle	m^2 [$(\mathrm{GeV/c^2})^2$]
π	$m^2 < 0.1$
K^+	$0.15 < m^2 < 0.5$
proton	$0.65 < m^2$

Here, ℓ is the path length to the TOF counter and Δt is the particle's time of flight. For this study, we smeared Δt with a gaussian σ_t of between 100 and 180 picoseconds. This σ_t is the expected timing resolution of a TOF counter and depends upon the scattering angle of the particle. In Fig. 3, we show the mass squared distributions of πs, K^+s and protons. Note the excellent separation of the mass peaks[3]. In Table 1 the selection criteria for identifying pions, kaons and protons are tabulated.

4.3 Invariant Mass

Because the target nucleon has substantial momentum due to fermi motion, the technique of missing mass (see eqn. 3) can only crudely distinguish the types of hyperons; the fermi motion smears the mass peaks. We have chosen the route of calculating the invariant mass from the particle's decay products. For example 64% of the time, a Λ^0 decays into a proton and a π^-. From the 4-momenta of these decay products we can identify the Λ^0:

$$m_{\Lambda^0} = \sqrt{(E_p + E_{\pi^-})^2 - \sum_{i=1}^{3}(p_p^i + p_{\pi^-}^i)^2} \qquad (2)$$

Employing this technique, the Λ^0 mass can be resolved to within 1 $\mathrm{MeV/c^2}$ for magnetic fields exceeding one quarter nominal strength. This method can also be applied to identifying the isospin triplet hyperons.

4.4 $\gamma + p \rightarrow \mathbf{K^+} + \Lambda^0$

We identify the Λ^0 by calculating the invariant mass from the decay products, the π^- and the proton. We invoke the following conditions for particle identification:

[3]Should σ_t degrade by a factor of two, our m^2 cuts will still clearly separate the low mass hadrons.

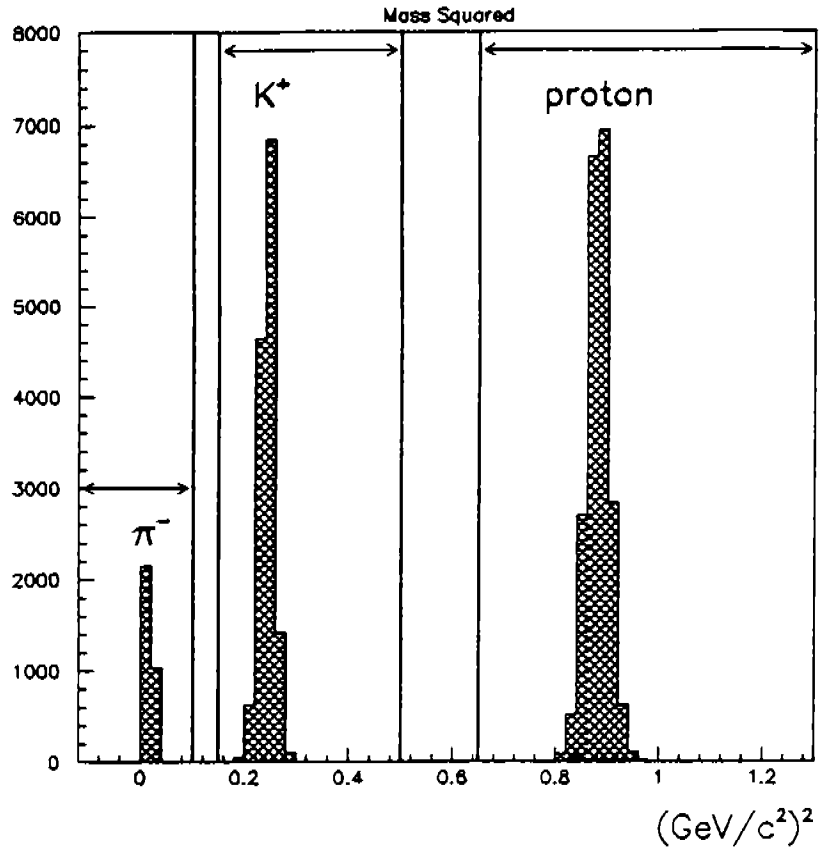

Figure 3: Mass squared distribution of π^-s, K^+s and protons. Here, $B = +0.5B_0$ and $E_\gamma = 1.5$ GeV.

- proton

    1. Positively charged
    2. Tracked through regions I, II & III and deposits energy in a TOF counter
    3. $m^2 > 0.65$ $(\mathrm{GeV/c^2})^2$

- π^-

    1. Negatively charged
    2. Tracked through at least regions I & II

If we were to demand that the pion make it through region III and strike a TOF counter, the acceptance would drop by a factor of three for a positive polarity field of half nominal strength. Reversing the field does not serve to improve the acceptance, for now the protons are swept toward the axis and are less likely to penetrate the scintillation counters. In Fig. 4, we show the invariant mass distribution of the proton and π^- for $\vec{B} = +0.5B_0$. From the fitted gaussian, we obtain a mass resolution of $\Delta m/m < 0.1\%$.

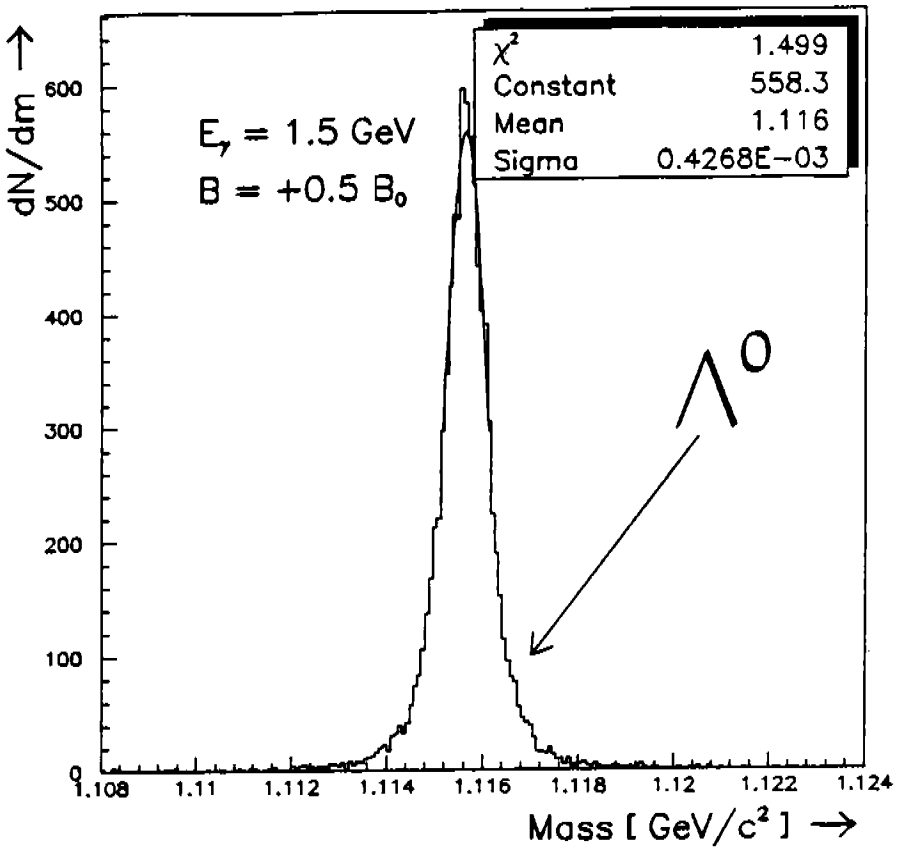

Figure 4: Invariant mass of proton and π^- from the reaction $p(\gamma, \Lambda^0)K^+$, where $\Lambda^0 \rightarrow p\pi^-$.

In Fig. 5 we plot the efficiency as a function of incident photon energy and magnetic field strength for reconstructing Λ^0. Similarly, in Figs. 6 and 7, we show the efficiency of measuring both the Λ^0 and K^+ in coincidence. Whereas in the former, K^+ need only be tracked in Regions I & II, in the latter K^+ must make it through all three regions and strike a TOF counter.

In Fig. 8, we compare the generated and accepted momentum distributions for the Λ^0.

4.5 $\gamma + p \rightarrow \mathbf{K^+} + \Sigma^0$

Σ^0 decays electromagnetically 100% of the time into a Λ^0 and a γ. We apply the following selection criteria for K^+ and the decay γ:

- K^+

  1. Positively charged
  2. Tracked through regions I, II & III and deposits energy in a TOF counter
  3. $0.15 < m^2 < 0.5$ $(GeV/c^2)^2$

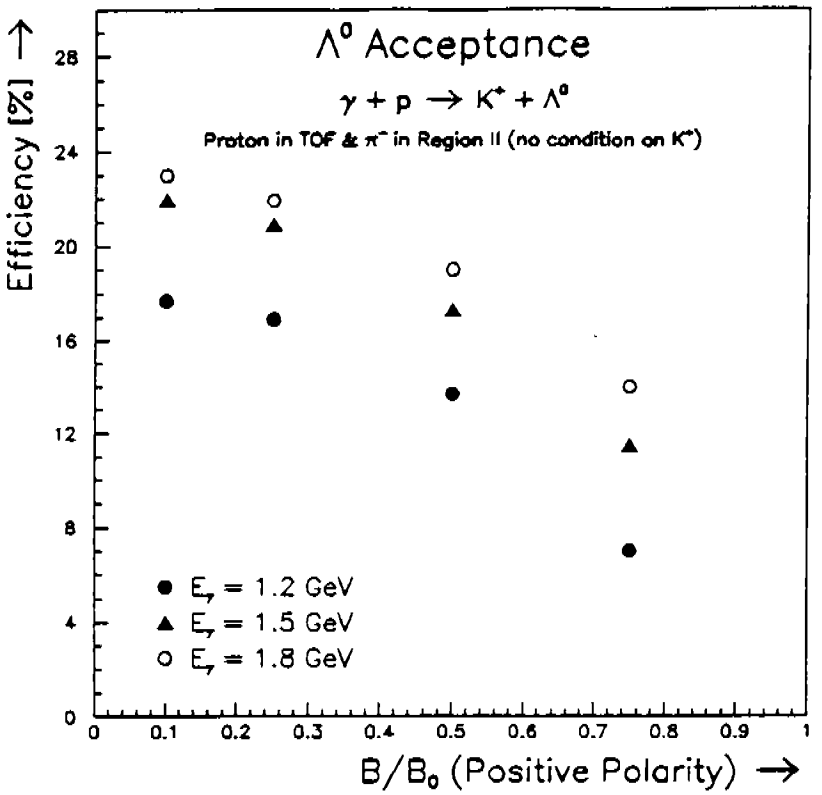

Figure 5: Acceptance as a function of E_γ and B/B_0 for Λ^0 in $p(\gamma,K^+)\Lambda^0$.

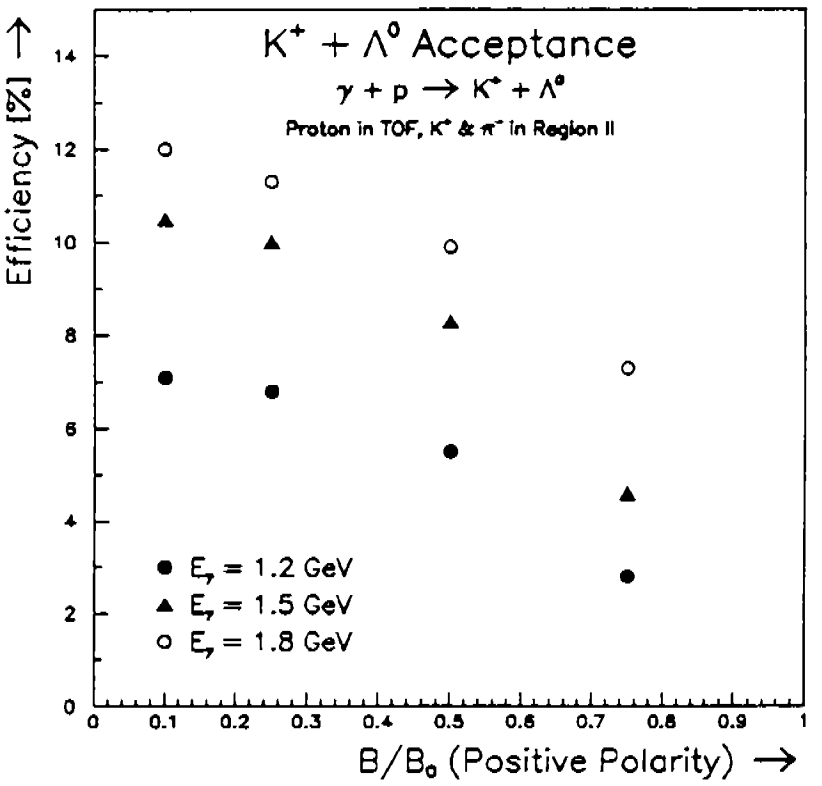

Figure 6: Acceptance as a function of E_γ and B/B_0 for Λ^0 and K^+ in coincidence in $p(\gamma,K^+\Lambda^0)$.

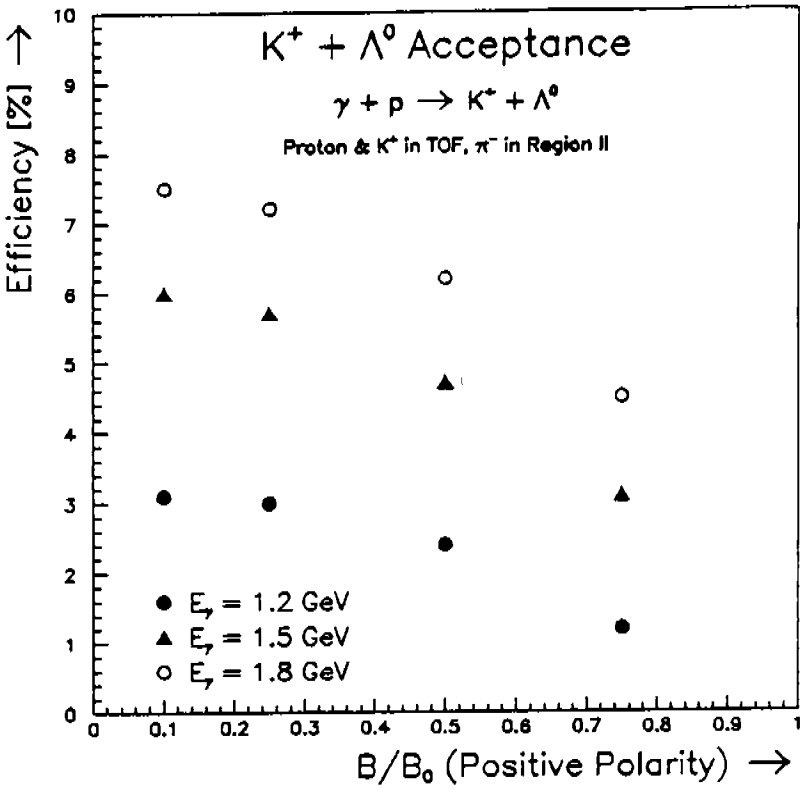

Figure 7: Acceptance as a function of E_γ and B/B_0 for $p(\gamma,K^+\Lambda^0)$.

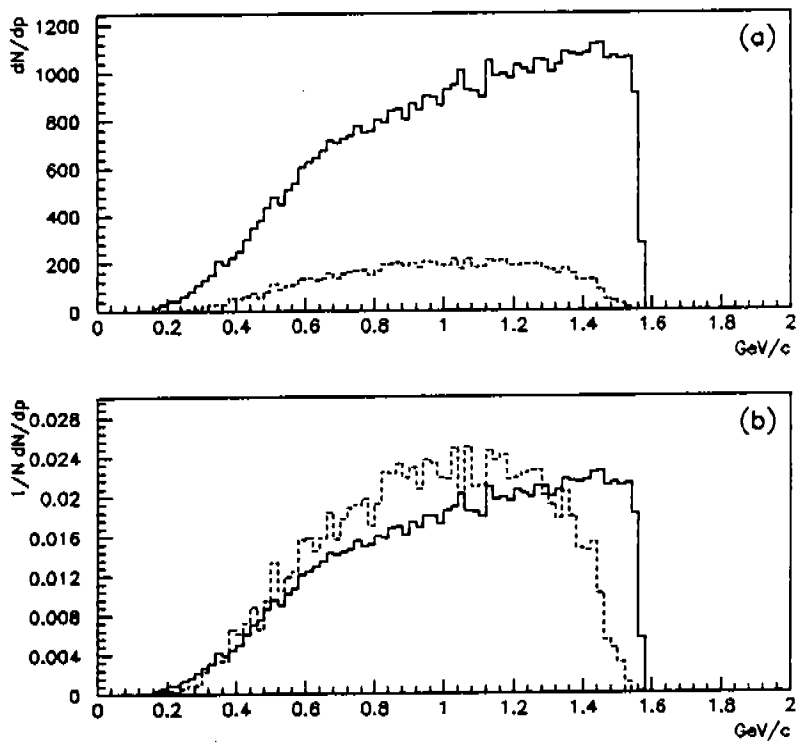

Figure 8: Comparison of the Λ^0 momentum distributions. (a) $\frac{dN}{dp}$ vs. p and (b) $\frac{1}{N}\frac{dN}{dp}$ vs. p where the solid line is the *Generated* and the dashed line is the *Accepted* distribution. ($B = +0.5B_o$, $E_\gamma = 1.5$ GeV).

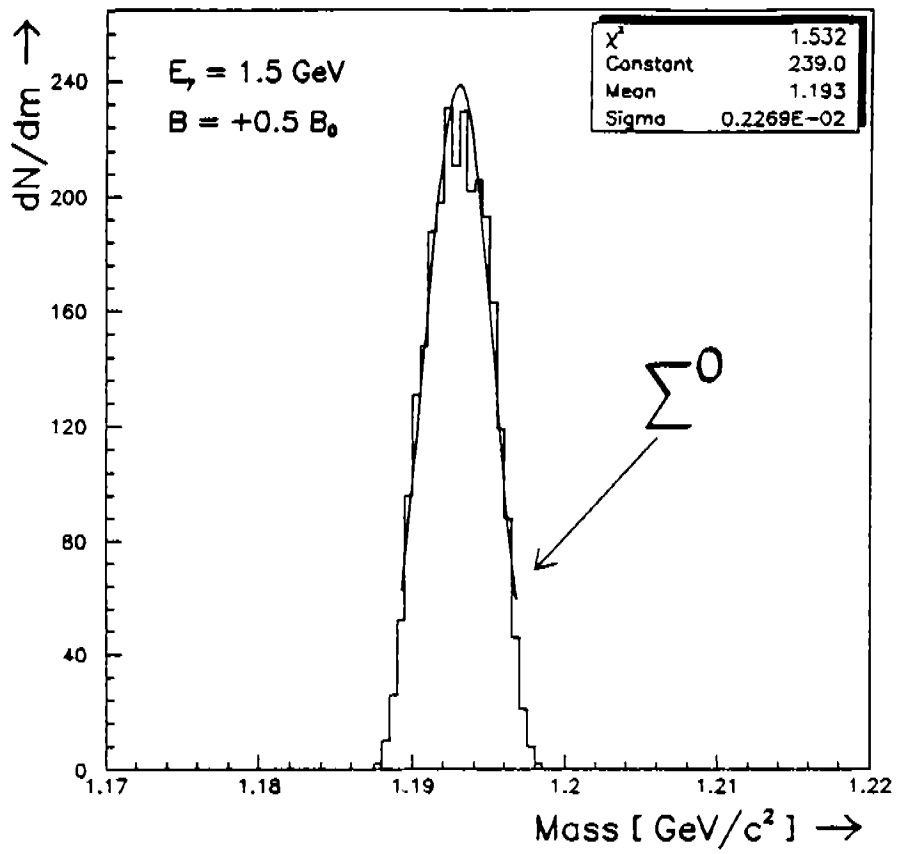

Figure 9: Invariant mass of Λ^0 and γ for the reaction $p(\gamma, \Sigma^0)K^+$, where $\Sigma^0 \rightarrow \Lambda^0\gamma$.

- decay γ

  1. Not tracked in regions I, II & III
  2. Deposits energy in an electromagnetic shower counter
  3. Time of flight less than 18 ns (i.e. $\beta = 1$)

The means by which the Λ^0 particle is identified is listed on page 9, i.e. we measure a proton in a TOF counter and a π^- is tracked through regions I & II. Fig. 9 shows the mass resolution of the Σ^0 formed from the 4-momenta of the decay products, γ and Λ^0, where the decay γ was uniformly smeared within the interval of $|\Delta p/p| \leq 7\%$. In Figs. 10(a) and 10(b), we plot the detection efficiency of $p(\gamma,K^+\Sigma^0)$ events as a function of tagged photon energy and magnetic field strength with varying conditions on K^+ acceptance. The field is reversed (positives bend toward the axis) in Figs. 11(a) and 11(b). Reversing the field tends to lower the acceptance for fields exceeding $0.25B_0$.

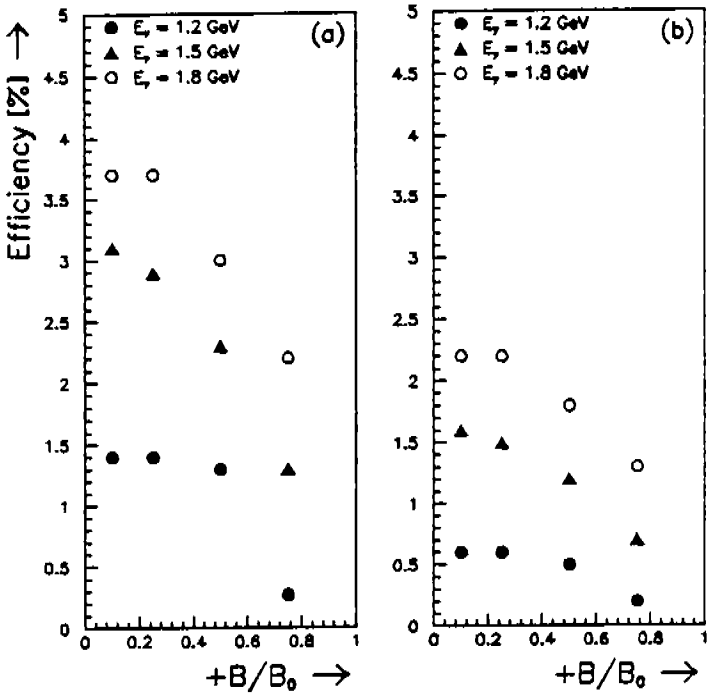

Figure 10: Acceptance as a function of E_γ and $+B/B_0$ for the decay γ, Λ^0 and K^+ in coincidence in the reaction $p(\gamma,K^+\Sigma^0)$ for (a) K^+ making through at least regions I & II and (b) K^+ making it through regions I, II & III and hitting TOF.

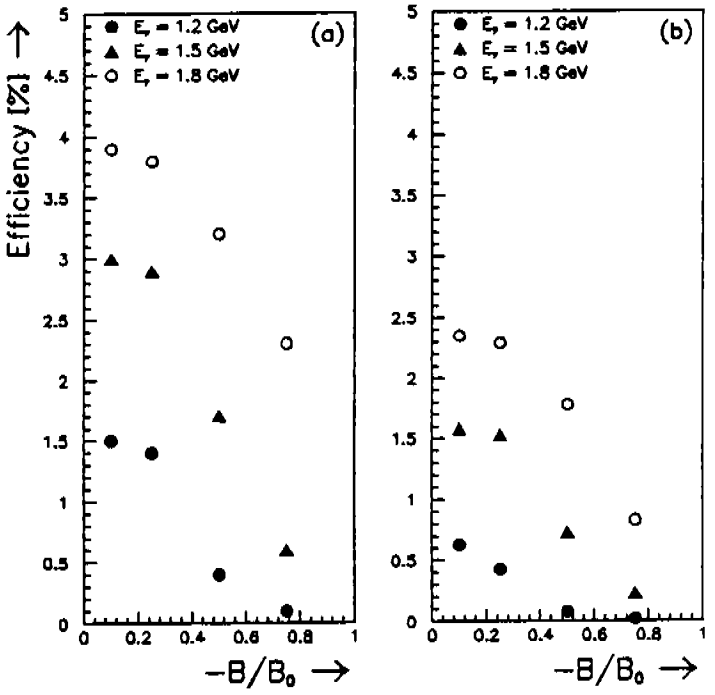

Figure 11: Acceptance as a function of E_γ and $-B/B_0$ for the decay γ, Λ^0 and K^+ in coincidence in the reaction $p(\gamma,K^+\Sigma^0)$ for (a) K^+ making through at least regions I & II and (b) K^+ making it through regions I, II & III and hitting TOF.

4.6 The Σ^0-Λ^0 Problem

The cuts listed in subsection 4.4 are necessary for accepting $p(\gamma,K^+\Lambda^0)$ events but not sufficient for separating Λ^0s arising from Σ^0 decay. For the case of the $p(\gamma,K^+\Sigma^0)$ reaction, the decay γ in the electromagnetic shower counter unambiguously tags the Σ^0. For $1.2 < E_\gamma < 1.8$, the ratio of reconstructed Λs from Σ^0 decay and primary Λs from $p(\gamma,K^+\Lambda^0)$ range from 60% to 86%, with the conditions $B = +0.5B_0$ and K^+ measured in TOF. Moreover, one out of every three Λs originating from Σ^0 decay is in coincidence with an accepted photon. *This fraction* is independent of beam energy or field strength. This implies 2/3 of these decay Λs are ambiguous, or between 29% and 36% of all accepted Λs are not primary.

We could employ the technique of missing mass to distinguish between Σ^0 and Λ^0 events that are in coincidence with a K^+, i.e.

$$m_Y = \sqrt{(E_\gamma + E_N - E_{K^+})^2 - (p^x_{K^+})^2 - (p^y_{K^+})^2 - (p^z_\gamma - p^z_{K^+})^2} \tag{3}$$

where $Y = (\Lambda^0, \Sigma^0)$, E_N is set to the mass of the nucleon since we cannot know the x, y, z components of the nucleon's fermi momentum and the momentum of the tagged photon is along the z axis. We need the experimental data to definitively ascertain how well the Λ^0 and the Σ^0 peaks can be separated. If we assume, however, that the events generated from the Monte Carlo roughly resemble reality, we can use this simulation to estimate how well we can distinguish these hyperon peaks. In Fig. 12 we plot the missing mass distributions for both Λ^0 and Σ^0. There is significant overlap. Subtracting the Σ^0 yield from the Λ^0 missing mass distribution and comparing this $\Lambda^0 - \Sigma^0$ distribution to the Λ^0 yield, we find that these two distributions agree to better than 80% until M_x exceeds 1.08 GeV/c^2. Fitting a gaussian to this Λ^0 missing mass distribution gives $\langle M_x \rangle = 1.142$, $\sigma_{M_x} = .073$ and $\chi^2_{dof} = 0.9$. This implies if we accept only events with $M_x < 1.142$ GeV/c^2, we throw out 50% of the Λ^0s. This will reduce the $p(\gamma,K^+\Lambda^0)$ acceptance to the 3% level (see Fig. 7), and is comparable to the $p(\gamma,K^+\Sigma^0)$ detection efficiency (Fig. 10) for $E_\gamma = 1.5$ GeV and $B = +0.25B_o$.

4.7 $\gamma + n \rightarrow K^+ + \Sigma^-$

Nearly 100% of the time, a Σ^- will decay into a neutron and a π^-. Because the proper decay length of the Σ^- is 4.4 cm, virtually all will have decayed before reaching region I.

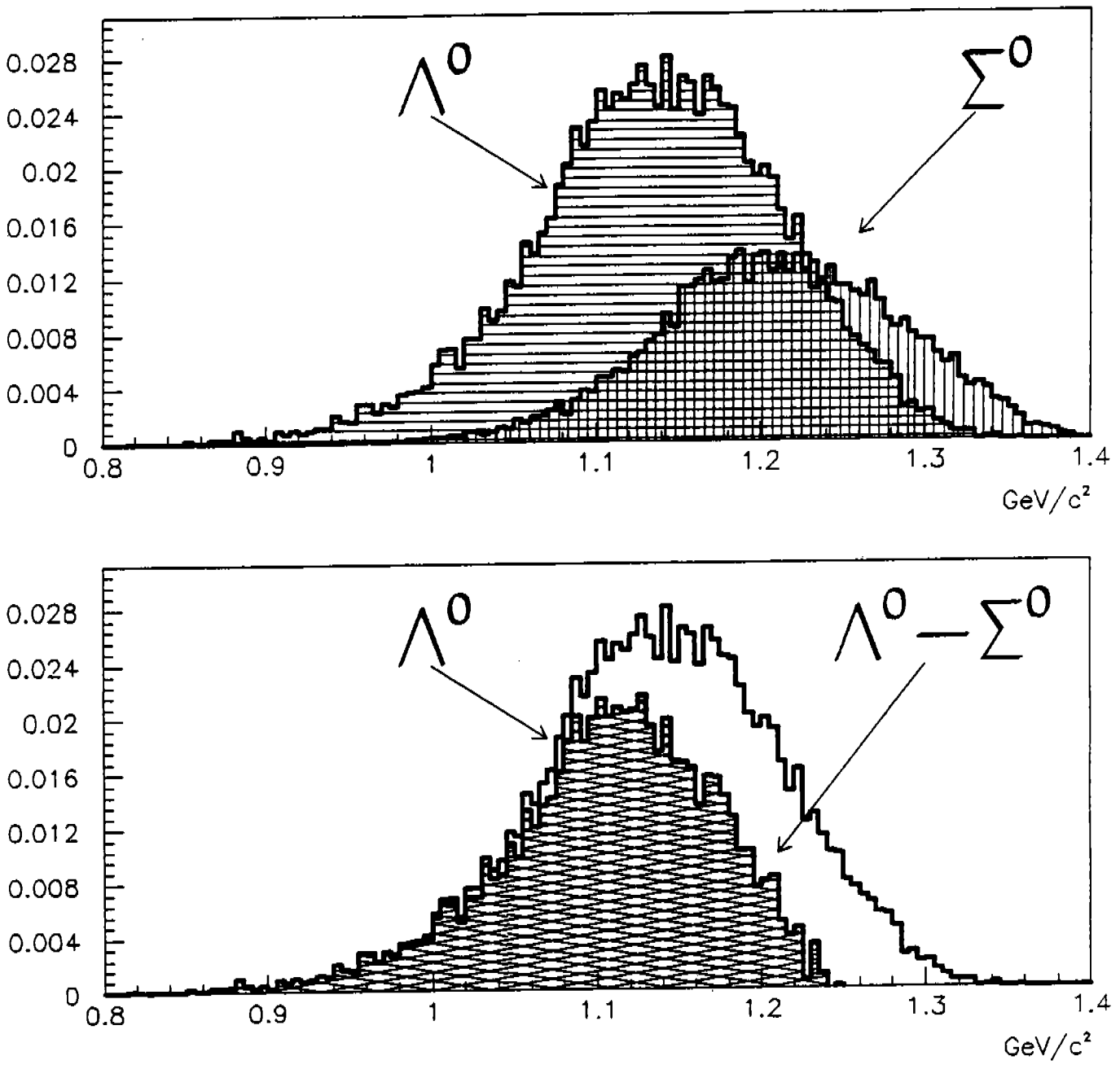

Figure 12: **(Above)** Hyperon missing mass for p(γ,K$^+$)Y. Horizontal (vertical) line interior denotes Λ^0 (Σ^0) mass distribution. Cross-hatched region refects the overlap. **(Below)** Λ^0 and $\Lambda^0 - \Sigma^0$ mass distributions. (B = $+0.5B_0$).

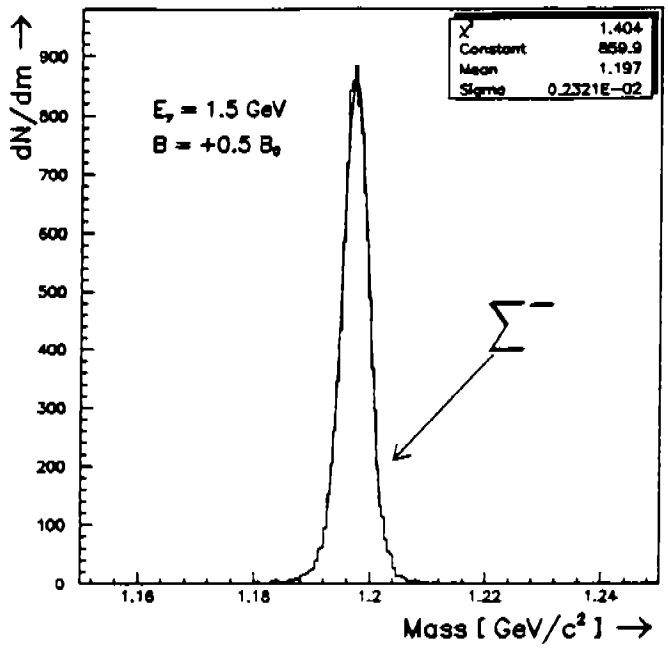

Figure 13: $n + \pi^-$ invariant mass distribution for $\Sigma^- \rightarrow n\pi^-$. ($B = +0.5B_0$).

We demand that the K^+ be particle identified and be in coincidence with the neutron and π. For the decay products of the Σ^-, we demand:

- π^-
  1. Negatively charged
  2. Tracked through regions I & II
- neutron
  1. Not tracked in regions I, II & III
  2. Deposits energy in an electromagnetic shower counter (threshhold energy > 50 MeV)
  3. Time of flight exceeds 20 ns (i.e. $\beta < 1$)

In Fig. 13, the invariant mass of the neutron and π^- is plotted, where the neutron momentum resolution has been set to 5% (spatial and timing resolution are approximately equal). In Fig. 14(a), we plot the efficiency as a function of tagged photon energy and field strength of positive polarity for reconstructing $p(\gamma,K^+\Sigma^-)$ events with the neutron, π^- and K^+ in coincidence. In Fig. 14(b), we reverse the field. As in the case for $p(\gamma,K^+\Sigma^0)$, reversing the field tends to degrade the acceptance for fields exceeding $0.25B_0$. Barring any untoward background effects, reconstructing the invariant

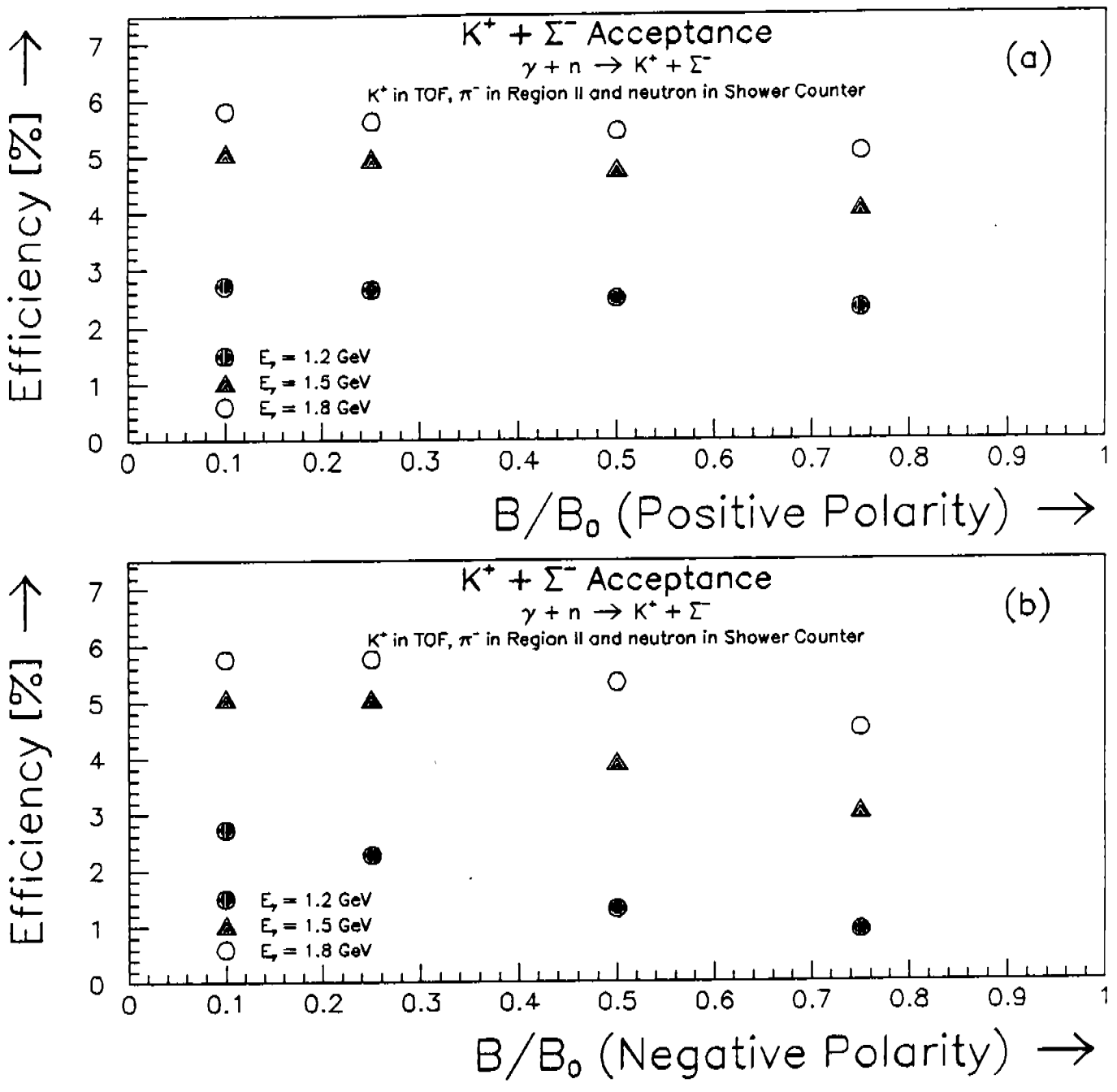

Figure 14: Acceptance as a function of E_γ and B/B_0 with Σ^- and K^+ in coincidence for the reaction $n(\gamma,K^+\Sigma^-)$ for (a) Positive polarity and (b) Negative polarity fields.

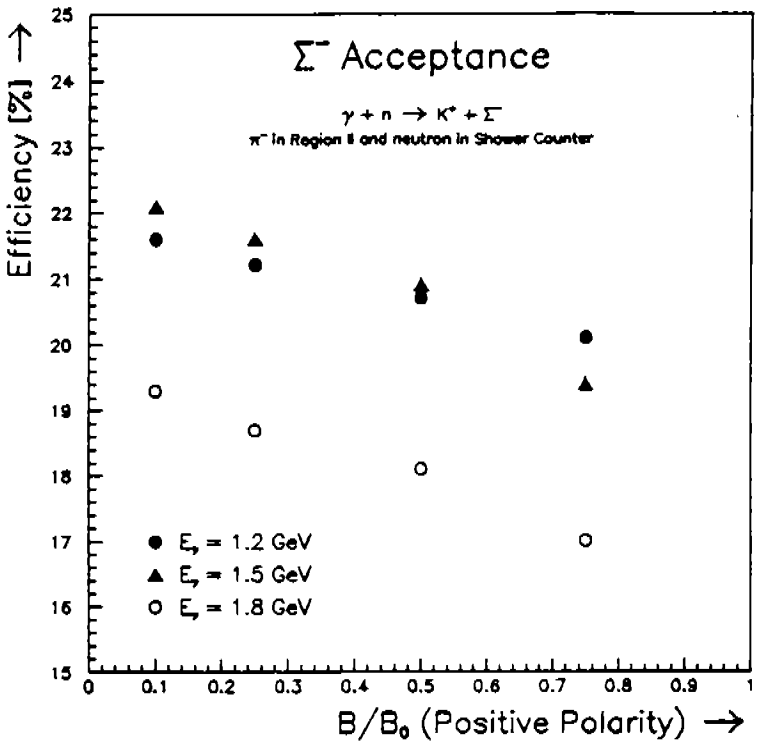

Figure 15: Σ^- acceptance as a function of E_γ and B/B_0 with no conditions on K^+ for the reaction $n(\gamma, \Sigma^-)K^+$.

mass from a neutron-π^- pair alone ought to unequivocally identify the Σ^-. Without the coincident K^+, the Σ^- acceptance attains the 20% level (See Fig. 15).

4.8 $\gamma + n \rightarrow K^0 + \Lambda^0$ and $\gamma + n \rightarrow K^0 + \Sigma^0$

K^0s consist of 50% K^0_S and 50% K^0_L. The CLAS detector is sensitive only to K^0_Ss— the proper decay length of K^0_Ls is far beyond the dimensions of the CLAS. Moreover, 68.6 percent of the time, the K^0_S decays into a $\pi^+\pi^-$ pair. However, since $\Lambda^0 \rightarrow p\pi^-$, we must clearly identify which π^- belongs to which parent strange hadron. We make the following cuts:

- We particle-identify a proton in a TOF counter, along with two negatively and one positively charged particles that pass through regions I & II.
- we reconstruct *both* a K^0 and a Λ^0 in the event where we set the mass cuts:
  1. $1.112 < m_{\Lambda^0} < 1.120$ GeV/c^2 (i.e. invariant mass of $p\pi^-$)
  2. $0.490 < m_{K^0} < 0.505$ GeV/c^2 (i.e. invariant mass of $\pi^+\pi^-$)

The mass distributions for coincident reconstructed K^0 and Λ^0 in an $n(\gamma,K^0\Lambda^0)$ event are plotted in Figs. 16(a) and 16(b). Similar plots for the reaction $n(\gamma,K^0\Sigma^0)$ are shown in Figs. 17(a) and 17(b). These cuts, however, are not sufficient to distinguish $n(\gamma,K^0\Lambda^0)$ from $n(\gamma,K^0\Sigma^0)$ and we should employ the technique of missing mass (eqn. 3) to separate the Σ^0 and Λ^0 events.

4.9 $\gamma + p \rightarrow K^0 + \Sigma^+$

The Σ^+ decays to either $n\pi^+$ (B.R. = 48.3%) or $p\pi^0$ (B.R. = 51.6%). We have investigated the former decay mode. The selection criteria for neutrons and pions have been detailed above. If the 4-momenta of the neutron and pion combine to form an invariant mass in the range of $1.182 < m_{\Sigma^+} < 1.196$ GeV/c^2, we say the event comes from the $p(\gamma,\Sigma^+)K^0$ channel (See Fig. 18). In Figs. 19(a) and 19(b) we plot the Σ^+ acceptance with and without the K^0 in coincidence. As in the case of Σ^- acceptance, the invariant mass criterion alone should suffice to determine the acceptance of the Σ^+ and one need not reconstruct the K^0.

4.10 K^0 & K^+ Acceptances

In Figs. 20(a) and 20(b) the K^+ and K^0 acceptances are plotted as a function of incident photon energy and magnetic field strength. These kaons originate from the reactions $N(\gamma,K\Lambda^0)$. The selection criteria for the K^+ (K^0) are described on p. 11 (p. 20). Note that the K^0 acceptance is nearly independent of E_γ and B/B_o. The CLAS detectors preferentially accept K^+s over K^0s by a factor ranging from 1.4 up to 2.7 depending on incident photon energy.

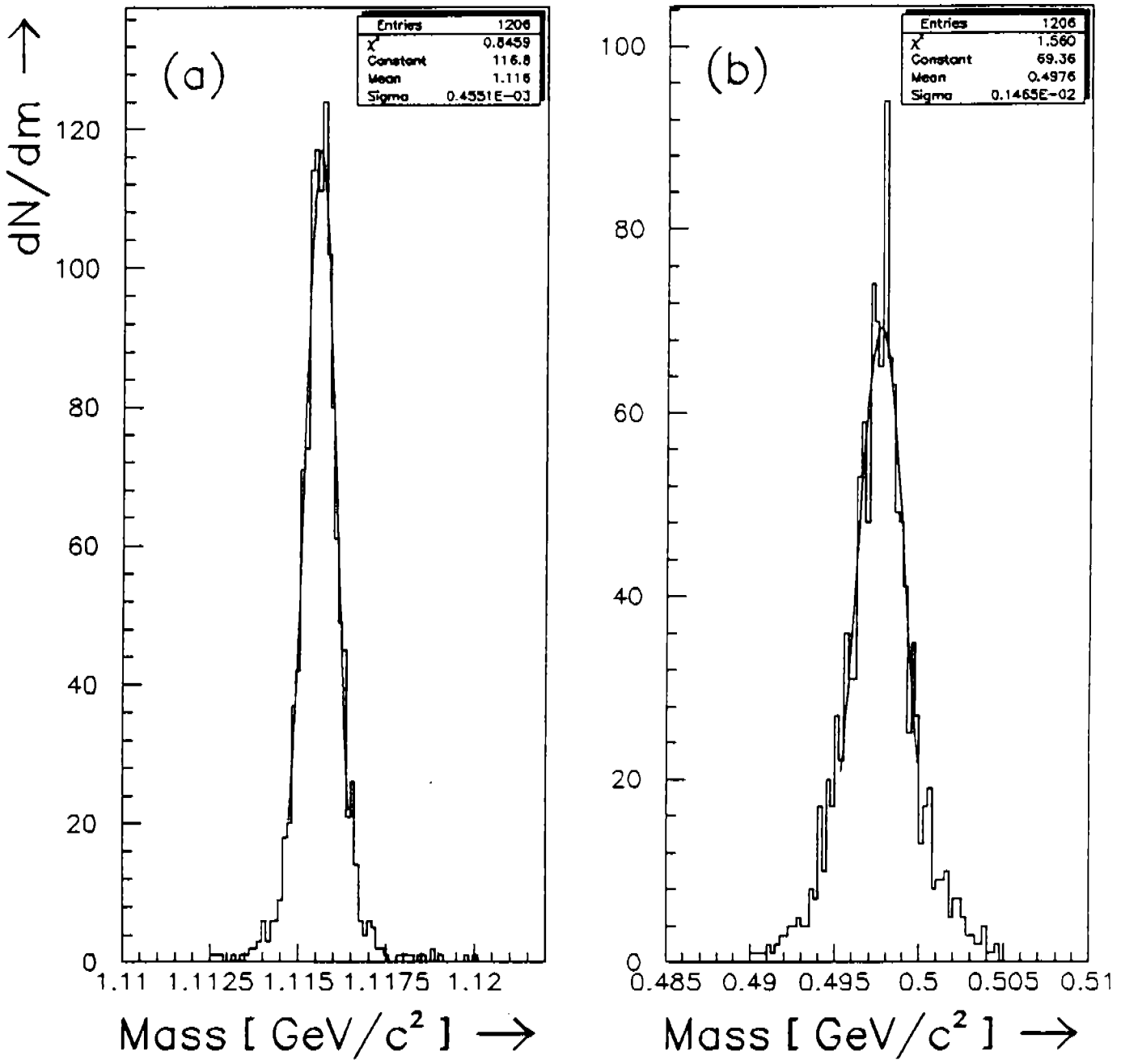

Figure 16: Mass distributions for (a) Λ^0 and (b) K^0 in the reaction n(γ,$K^0\Lambda^0$).

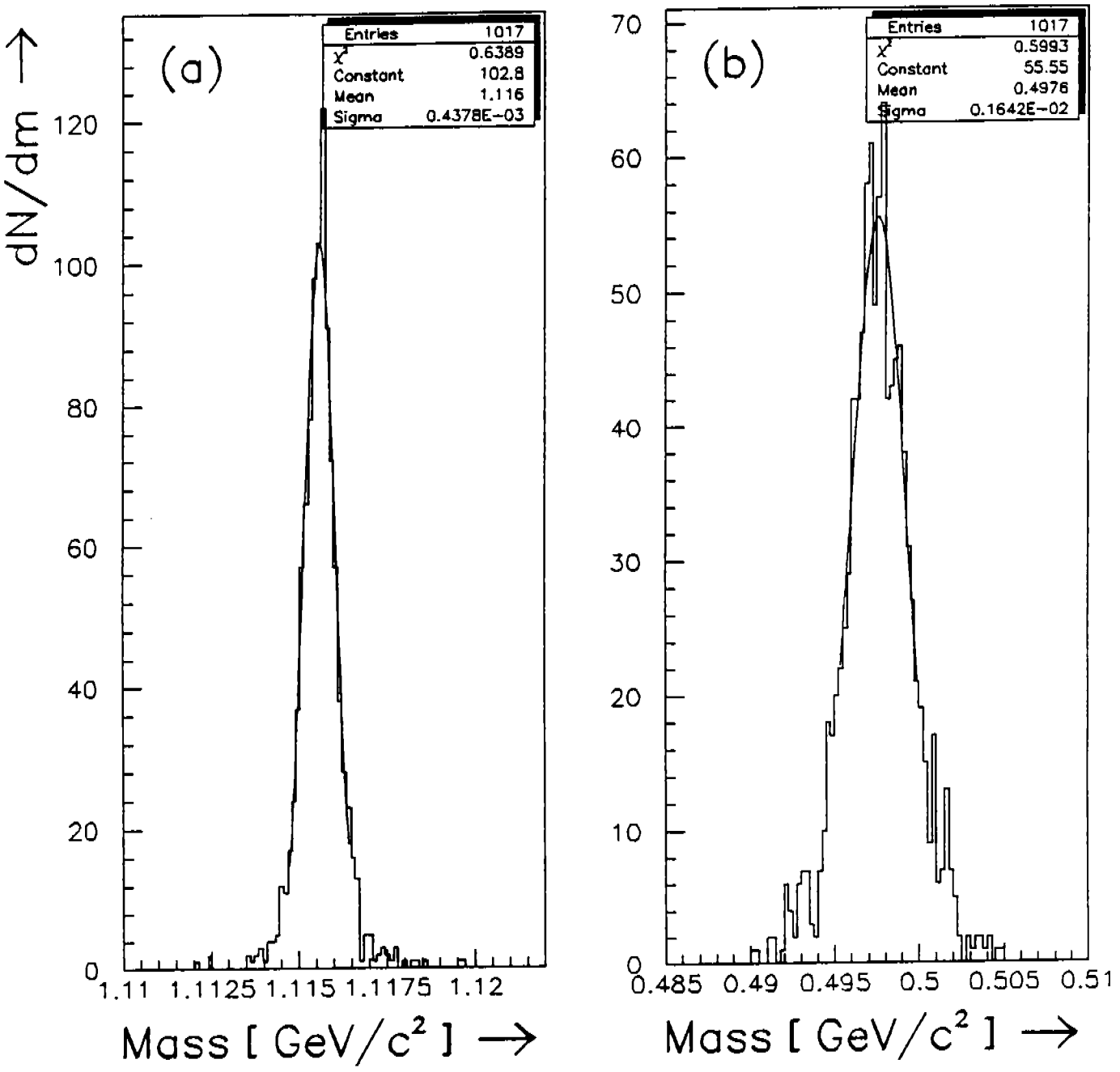

Figure 17: Mass distributions for (a) Λ^0 and (b) K^0 in the reaction $n(\gamma,K^0\Sigma^0)$. (K^0 and Λ^0 both reconstructed in the event.)

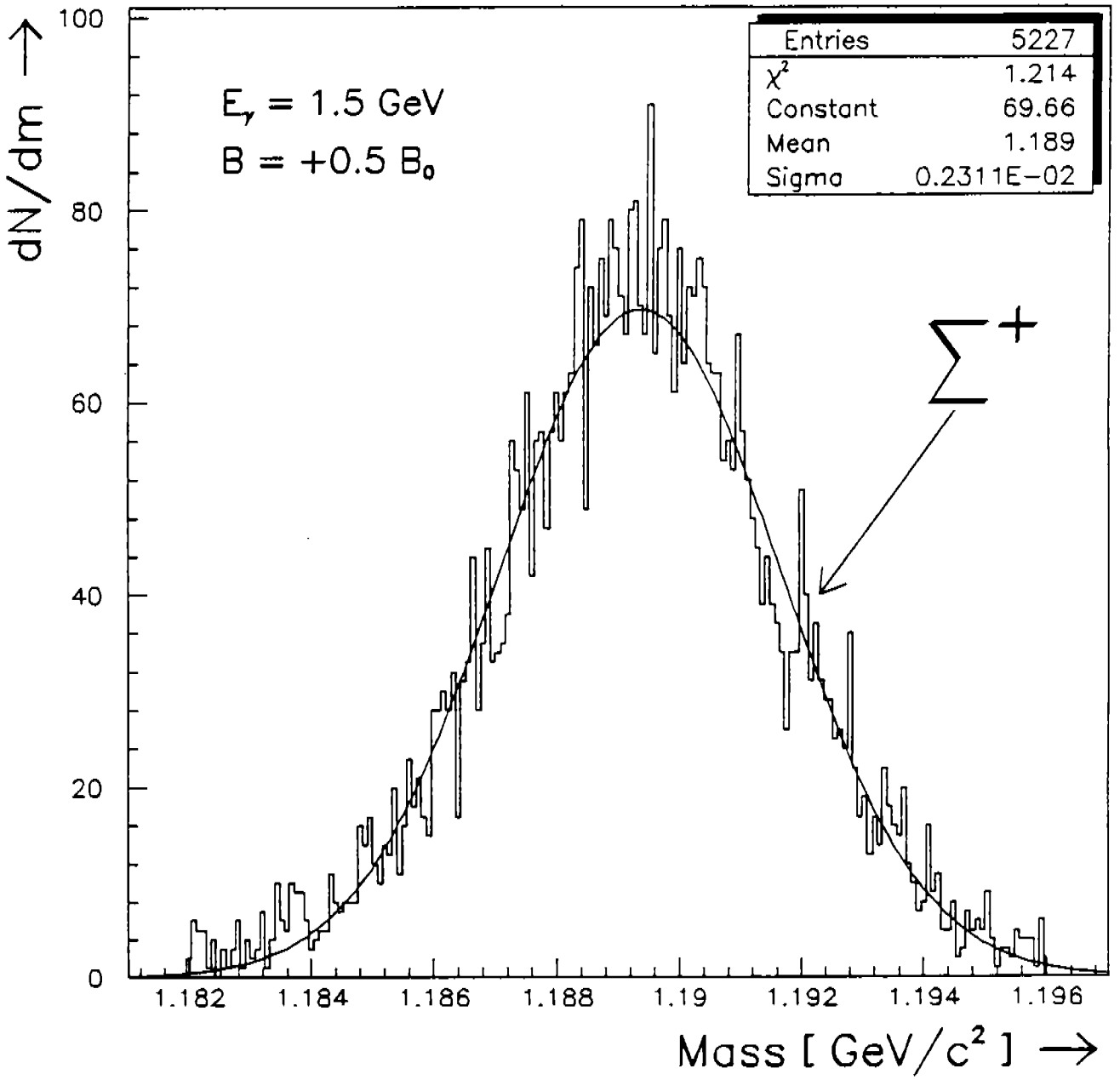

Figure 18: Invariant mass distribution of $n\pi^+$ in Σ^+ decay.

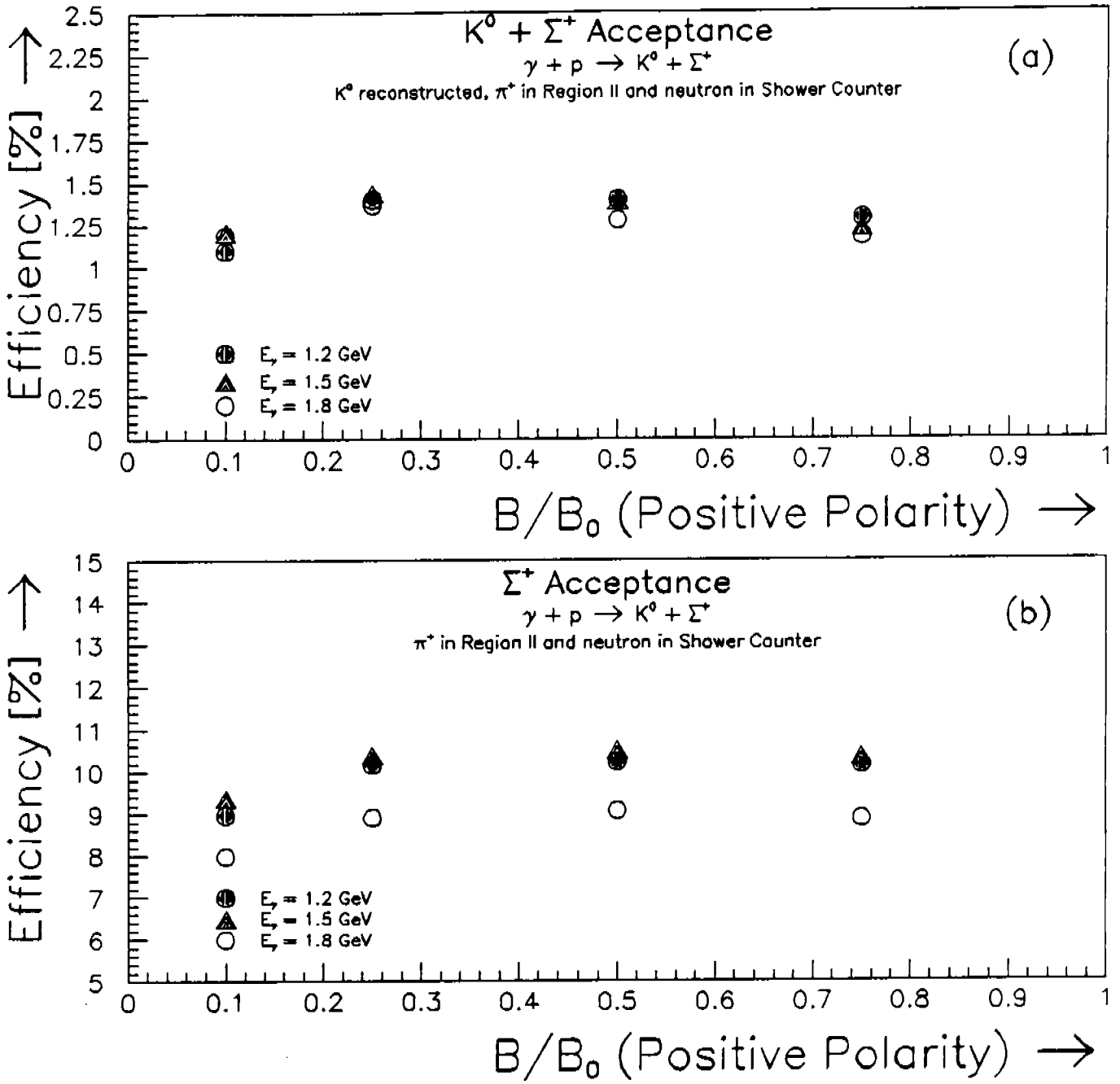

Figure 19: Acceptance as a function of E_γ and B/B_0 for Σ^+ (a) K^0 in coincidence and (b) K^0 *not* in coincidence.

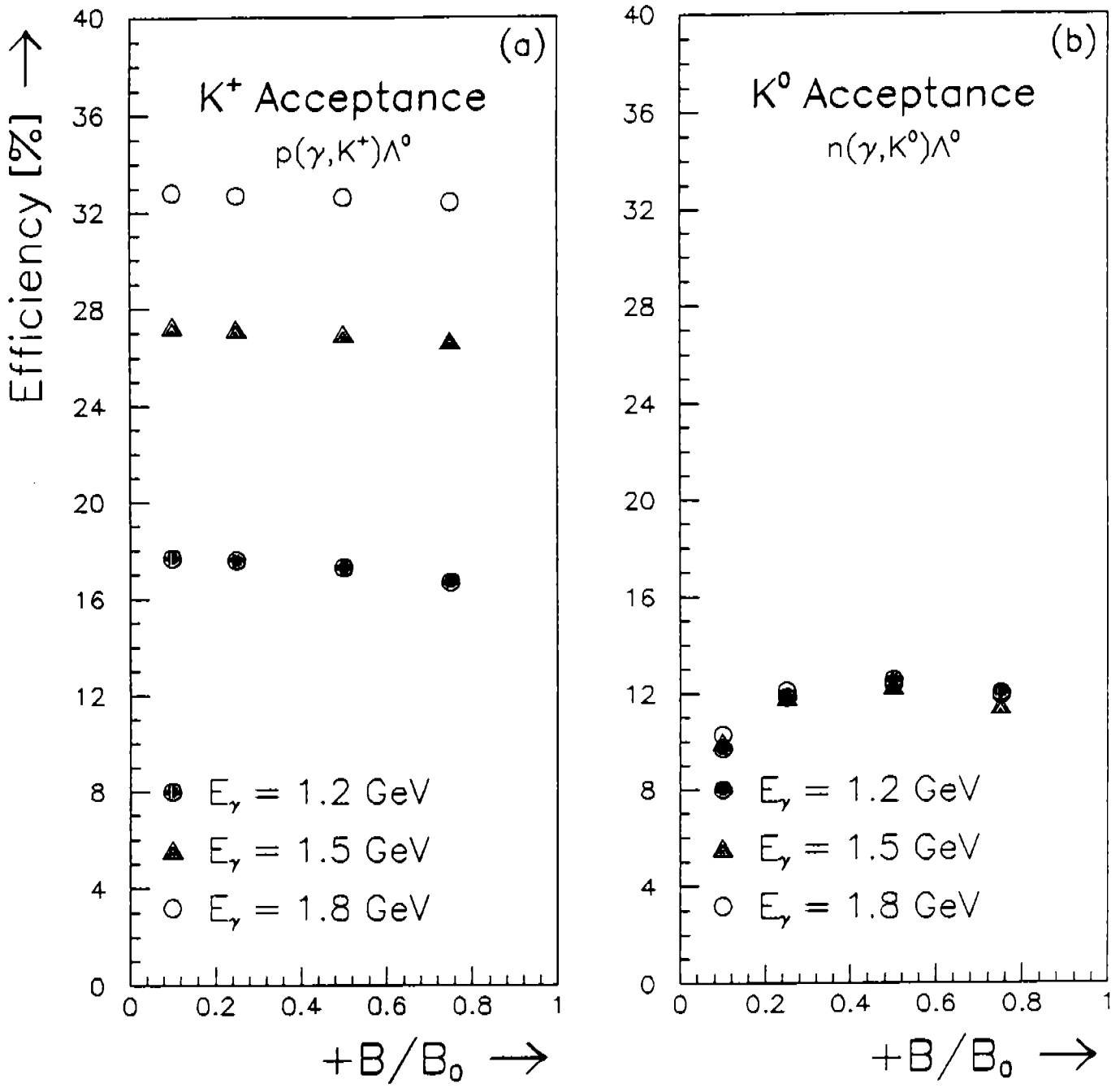

Figure 20: (a) K^+ acceptance from the reaction $p(\gamma,K^+)\Lambda^0$ and (b) K^0 acceptance from the reaction $n(\gamma,K^0)\Lambda^0$.

5 Future Improvements and Refinements

In the above acceptance calculations we have striven to precisely identify from which KY channels the strange particles originate. Demanding that a kaon be in coincidence with a hyperon reduces the acceptance to the $\sim 5\%$ ($\sim 2.5\%$) level for the K^+ (K^0) channels. Further restrictions naturally degrade the acceptance, e.g. that we detect both the γ and Λ^0 in Σ^0 decay reduces the acceptance by 66%.

In this section we discuss the detection efficiencies of decay modes not studied above and the effects of relaxing our draconian cuts. Besides the $p\pi^-$ branch, the Λ^0 hyperon can decay into a $n\pi^0$. This π^0 then decays into two γs. What are the detection efficiencies, then, for accepting the neutron in coincidence with either one or both γs or without any γs in coincidence at all? In Tables 2 and 3 we address this issue. In the first column we list the hyperon under study. The decay modes are tabulated in column II, where the quantities in parentheses are the efficiencies of not detecting the particles. The total acceptance, then, is:

$$\text{Acceptance} = \text{B.R.} \times \prod \varepsilon_i$$

where B.R. is the branching ratio and $\prod \varepsilon_i$ is the total efficiency of measuring the π and γ decay products in or *not* in coincidence with the decay nucleon.

A K^+ is created in coincidence with a Λ^0, Σ^0 or a Σ^- hyperon. These hyperons have the following decay modes (see Table 2), where the the underlined decay modes have been studied above:

- Λ^0
  - $\underline{\Lambda^0 \rightarrow p\pi^-}$ (64.1%)
  - $\Lambda^0 \rightarrow n\pi^0$ (35.7%) and $\pi^0 \rightarrow \gamma\gamma$ ($\sim 100\%$)
- $\Sigma^0 \rightarrow \Lambda^0\gamma$
  - $\underline{\Sigma^0 \rightarrow p\pi^-\gamma}$ (64.1%)
  - $\Sigma^0 \rightarrow n\pi^0\gamma$ (35.7%) and $\pi^0 \rightarrow \gamma\gamma$
- Σ^-
  - $\underline{\Sigma^- \rightarrow n\pi^-}$ ($\sim 100\%$)

Table 2: Acceptance of hyperon decay products for B = $+0.25B_o$ E_γ = 1.5 GeV. Quantities in parentheses (col. II) correspond to the efficiencies of *not* detecting the particle.

Hyperon	Decay Mode	B.R.	$\prod\epsilon_i$	Acceptance = B.R. $\times \prod\epsilon_i$
Λ^0	$p\pi^-$	.64	(.63)(.53)	.21
	$p(\pi^-)$	.64	(.63)(.47)	.19
	$n\gamma\gamma$	.36	$(.34)(.34)^2$	.01
	$n\gamma(\gamma)$	.36	(.34)(.66)(.34)	.03
	$n(\gamma\gamma)$	.36	$(.34)(.66)^2$	.05
Σ^0	$p\pi^-\gamma$	.64	(.55)(.53)(.34)	.07
	$p\pi^-(\gamma)$	.64	(.55)(.53)(.66)	.12
	$p(\pi^-\gamma)$	.64	(.55)(.47)(.66)	.11
	$n\gamma\gamma\gamma$	.36	$(.34)(.34)^3$	$< .005$
	$n\gamma\gamma(\gamma)$	.36	$(.34)(.34)^2(.66)$	.01
	$n\gamma(\gamma\gamma)$	.36	$(.34)(.34)(.66)^2$	.02
	$n(\gamma\gamma\gamma)$	.36	$(.34)(.66)^3$	.04
Σ^-	$n\pi^-$	1.0	(.36)(.64)	.23
	$n(\pi^-)$	1.0	(.36)(.36)	.13

Like the K^+, for the neutral channels the K^0 is created in coincidence with either the Λ^0 or Σ^0 and we have listed the decay modes above. The K^0 can also be accompanied with a Σ^+ hyperon (see Table 3).

- Σ^+
  - $\underline{\Sigma^+ \rightarrow n\pi^+}$ (48.3 %)
  - $\Sigma^+ \rightarrow p\pi^0$ (51.6%) and $\pi^0 \rightarrow \gamma\gamma$

Table 3: Acceptance of hyperon decay products for B = $+0.25B_o$ E_γ = 1.5 GeV. Quantities in parentheses (col. II) correspond to the efficiencies of *not* detecting the particle.

Hyperon	Decay Mode	B.R.	$\prod\epsilon_i$	Acceptance = B.R. $\times \prod\epsilon_i$
Λ^0 and Σ^0	*Same as for* K^+			
Σ^+	$n\pi^+$	.48	(.36)(.60)	.10
	$n(\pi^+)$	.48	(.36)(.40)	.07
	$p\gamma\gamma$	.52	$(.57)(.34)^2$	.03
	$p\gamma(\gamma)$	.52	(.57)(.34)(.66)	.07
	$p(\gamma\gamma)$	.52	$(.57)(.66)^2$	.13

6 Summary

In this CLAS note we have investigated the detection efficiencies of photoproduced strange particles for the six N(γ,KY) reactions. We find the high acceptance of the CLAS eminently well suited for hyperon experiments. We have shown that our techniques for reconstructing hyperons and kaons are general and do not depend upon whether the photon is real or virtual and are nearly independent of target.

We have, however, not included such effects as background, track reconstruction inefficiencies and the potential problems arising from misidentifying μs as πs. Such studies require a GEANT based detector simulation package. In section 5 we discussed additional hyperon signatures that may well increase the KY acceptance. Such an endeavor is worthy of study and will be covered in a future CLAS note.

7 Acknowledgments

I wish to thank Charles Hyde-Wright and Elton Smith for their help in this study and I appreciate my many fruitful discussions with Barry Berman.

References

[1] CEBAF proposal, "Quasi-Free Strangeness Production in Nuclei," PR-91-014
(Spokesman: Charles E. Hyde-Wright)

[2] Elton S. Smith, "FAST Monte Carlo Program for the CLAS Detector, CLAS-NOTE 90-003

[3] Charles E. Hyde-Wright, private communication